LA-UR-97-3918

CONF-980635--

Los Alamos National Laboratory is operated by the University of California for the United States Department of Energy under contract W-7405-ENG-36



TITLE: **DIRECT NUMERICAL SIMULATION OF SOLIDIFICATION MICROSTRUCTURES AFFECTED BY FLUID FLOW**

AUTHOR(S): Damir Juric, T-3



SUBMITTED TO: To be presented at the *Modeling of Casting, Welding and Advanced Solidification Processes VIII Workshop*, San Diego, CA, June 7-12, 1998.



Los Alamos

Los Alamos National Laboratory
Los Alamos, New Mexico 87545

FORM NO. 836 R4
ST. NO. 2629 5/81

## DISCLAIMER

# DIRECT NUMERICAL SIMULATION OF SOLIDIFICATION

# MICROSTRUCTURES AFFECTED BY FLUID FLOW

Damir Juric

Theoretical Division, MS B216
Los Alamos National Laboratory
Los Alamos, New Mexico 87545

Abstract

The effects of fluid flow on the solidification morphology of pure materials and solute microsegregation patterns of binary alloys are studied using a computational methodology based on a front tracking/finite difference method. A general single-field formulation is presented for the full coupling of phase change, fluid flow, heat and solute transport. This formulation accounts for interfacial rejection/absorption of latent heat and solute, interfacial anisotropies, discontinuities in material properties between the liquid and solid phases, shrinkage/expansion upon solidification and motion and deformation of the solid. Numerical results are presented for the two-dimensional dendritic solidification of pure succinonitrile and the solidification of globulitic grains of a Plutonium-Gallium alloy. For both problems, comparisons are made between solidification without fluid flow and solidification within a shear flow.

## Introduction

Nearly all materials of engineering interest have, at some point, solidified from a liquid state. The exact nature of the solidification process determines the microstructure and thus the physical properties of the solid material. In most solidification situations some degree of fluid motion exists, whether by buoyant natural convection or forced convection due to electromagnetic stirring or some mechanical motion. Fluid motion may also be induced by the shrinkage or expansion of the solid upon solidification. In Czochralski crystal growth, solidification occurs at the end of a rotating rod as it is pulled from a crucible containing the melt. In rheocasting, a semi-solid charge of slurry is injected into a die where it deforms to the internal die shape before complete solidification. Convection in weld pools is driven by buoyancy, Lorentz and capillary forces. From these few examples it is clear that an understanding of how the fluid motion affects the dynamics of the solidification process and the resulting microstructure is crucial to many manufacturing technologies.

A variety of numerical methods have been successful in capturing the essential features of microscale solidification dynamics and morphologies of both pure materials and alloys. Some recent examples include finite element based [1–3], phase-field [4–8] and front-tracking [9, 10] methods. However, until recently these methods have only been applied to the problem without fluid convection. A notable extension of the phase-field method to include convection has just recently been developed by Diepers, Beckermann and Steinbach [11]. They used this method for direct simulations of microstructure formation in solidifying alloys. A front-tracking method for phase change problems including convection has also recently been developed for calculations of boiling flows [12]. As will be described below, this front-tracking method can be directly applied to the solidification of pure materials. With the addition of a solute transport equation the method can be extended to alloy solidification. The goal of this article is to describe the extension and generalization of the front tracking method to include solute transport and to apply the method to direct simulations of solidification microstructures in both pure materials and alloys with and without fluid convection. The formulation accounts for interfacial rejection/absorption of latent heat and solute, interfacial anisotropies, discontinuities in material properties between the liquid and solid phases and shrinkage/expansion upon solidification. In addition the method allows for arbitrarily complex deformations of the solid-liquid interface, topology changes and solid body motion and deformation.

The mathematical formulation and a brief description of the numerical method are presented in the next section. The subsequent section then presents numerical results for the two-dimensional dendritic solidification of pure succinonitrile and the solidification of globulitic grains of a Plutonium-Gallium alloy. Comparisons are made for the growth dynamics of the pure material and solute microsegregation in the binary alloy in a shear flow and also with no flow.

## Mathematical Formulation

We write a single set of conservation equations for the transport of mass, momentum, energy and species for the entire domain including the solid and liquid phases. The phase boundary is treated as an imbedded interface by adding to these conservation laws the appropriate source terms for surface tension, interphase mass transfer, jumps in material properties and rejection/absorption of latent heat and solute. These source terms are in the form of delta functions localized at the interface and are selected in such a way as to

satisfy the correct jump conditions across the phase boundary. The formulation presented here follows closely that of Juric and Tryggvason [12] for boiling flows except here we include the equation for solute transport.

We begin by specifying the material properties which are considered to be constant but not generally equal for each phase. As a consequence, the bulk phases are incompressible but we allow for volume expansion or shrinkage at the phase interface due to the density change upon solidification. Equations for the material property fields can be written for the entire domain using an indicator function, $I(\mathbf{x},t)$, which has the value 1 in the solid phase and 0 in the liquid phase. $I$ is similar to the phase-field variable in the phase field method, however here, as will be shown below, we determine $I$ from the known position of the tracked interface rather than use it to determine the position of the interface. The values of the material property fields at every location are given by $b(\mathbf{x},t) = b_L + (b_S - b_L)\, I(\mathbf{x},t)$, where the subscripts $S$ and $L$ refer to the solid and liquid phases respectively. $b$ stands for density, $\rho$, viscosity, $\mu$, specific heat, $c$, thermal conductivity, $k$ or diffusivity, $D$. Since $I$ is constant except in a local region near the interface, we can express the gradient of $I$ as a local surface integral

$$\nabla I = \int_{\Gamma(t)} \mathbf{n}\, \delta\left(\mathbf{x} - \mathbf{x}_i\right) ds\,, \tag{1}$$

where $\mathbf{n}$ is the unit normal to the interface, defined to point into the solid phase and $\mathbf{x}_i = \mathbf{x}(s,t)$ is a parameterization of the phase interface, $\Gamma(t)$. $\delta\left(\mathbf{x} - \mathbf{x}_i\right)$ is a three-dimensional delta function that is non-zero only where $\mathbf{x} = \mathbf{x}_i$. Taking the divergence of Eq. (1) results in

$$\nabla^2 I = \nabla \cdot \int_{\Gamma(t)} \mathbf{n}\, \delta\left(\mathbf{x} - \mathbf{x}_i\right) ds\,. \tag{2}$$

Thus we find $I(\mathbf{x},t)$ by solving the above Poisson equation where the right hand side is a function only of the known interface position at time $t$. The interface is advected in a Lagrangian fashion by integrating $(d\mathbf{x}_i/dt) \cdot \mathbf{n} = V_n = \mathbf{V} \cdot \mathbf{n}$. $\mathbf{V}$ is the interface velocity vector and $V_n$ its normal component. We assume that the tangential components of the interface velocity, $V$, and material velocity, $\mathbf{u}$, at the interface are equal, *i.e.* no slip at the interface.

With the aid of Eq. (1) and the definition of $\rho$, the conservation of mass for the entire domain can be expressed as

$$\nabla \cdot \rho\mathbf{u} = -\frac{\partial \rho}{\partial t} = \mathbf{V} \cdot \nabla \rho = \int_{\Gamma(t)} \left(\rho_S - \rho_L\right) V_n \delta\left(\mathbf{x} - \mathbf{x}_i\right) ds\,. \tag{3}$$

The momentum equation, in conservative form, is

$$\frac{\partial \rho\mathbf{u}}{\partial t} + \nabla \cdot \rho\mathbf{u}\mathbf{u} = -\nabla P - \rho\mathbf{g} + \nabla \cdot \boldsymbol{\tau} + \int_{\Gamma(t)} \gamma\kappa\mathbf{n}\delta\left(\mathbf{x} - \mathbf{x}_i\right) ds\,, \tag{4}$$

where $P$ is the pressure, $\mathbf{g}$ is the gravitational force, $\gamma$ is the surface tension coefficient (assumed constant in this equation), $\kappa$ is twice the mean interface curvature and $\boldsymbol{\tau}$ is the deviatoric stress tensor for a Newtonian fluid $\boldsymbol{\tau} = \mu\left(\nabla\mathbf{u} + \nabla\mathbf{u}^T\right)$. Note that we use this same constitutive relation for both the solid and liquid and make the assumption that the solid is a very viscous liquid. In this way we obtain a crude constitutive material model for the solid which allows solid motion and deformation.

The thermal energy equation with an interfacial source term to account for liberation or absorption of latent heat, $L$, is

$$\frac{\partial \rho c T}{\partial t} + \nabla \cdot \rho \mathbf{u} c T = -\nabla \cdot \mathbf{q} + \int_{\Gamma(t)} \dot{m} \left[ L + (c_L - c_S) T_{\text{sat}} \right] \delta (\mathbf{x} - \mathbf{x}_i) \, ds \tag{5}$$

where we have neglected the viscous dissipation. We assume that the constitutive relation for the heat flux, $\mathbf{q} = -k \nabla T$, holds throughout the entire domain. $T$ is the temperature and $\dot{m}$ is the interfacial mass flux, $\dot{m} = \rho_L (\mathbf{V} - \mathbf{u}_L) \cdot \mathbf{n} = \rho_S (\mathbf{V} - \mathbf{u}_S) \cdot \mathbf{n}$ .

The single-field solute transport equation is

$$\frac{\partial \rho \tilde{C}}{\partial t} + \nabla \cdot \rho \mathbf{u} \tilde{C} = \nabla \cdot \rho \tilde{D} \nabla \tilde{C} + \int_{\Gamma(t)} (1 - k) \dot{m} \tilde{C}_i \delta (\mathbf{x} - \mathbf{x}_i) \, ds \, , \tag{6}$$

where $\tilde{C}$ and $\tilde{D}$ are defined by the simple transformation for the solute concentration, $C$, [2] and diffusivity, $D$,

$$\left( \tilde{C}, \tilde{D} \right) = \begin{cases} (C_S/k, k D_S) \, , & \text{in the solid,} \\ (C_L, D_L) \, , & \text{in the liquid .} \end{cases} \tag{7}$$

The integral on the right hand side of Eq. (6) accounts for rejection or absorption of solute at the interface due to the difference in miscibility of the alloy components in the liquid and solid. $\tilde{C}_i = \tilde{C}(\mathbf{x}_i)$ is the value of the transformed concentration at the interface. Note that the transformed concentration is continuous at the interface which makes $\tilde{C}_i$ more easy to calculate numerically. In using this transformation the partition coefficient, $k = C_S(\mathbf{x}_i)/C_L(\mathbf{x}_i)$, is assumed to be constant which, for dilute mixtures, is usually a reasonable assumption. Since the interface is explicitly tracked and thus $I$ is known we can regain the original concentration field from $C = \tilde{C} + \left( k\tilde{C} - \tilde{C} \right) I(\mathbf{x})$.

It is important to recognize that away from the interface the single field formulation, Eqs. (3), (4), (5) and (6), reduces to the customary mass, momentum, thermal energy and solute equations for each of the bulk phases while integration of these equations across the interface reveals that the formulation naturally incorporates the correct mass, momentum, energy and solute balances across the interface. We have made the assumptions that the interface is thin and massless, the energy contribution due to interface stretching is negligible and the temperatures of the solid and liquid at the interface are equal. In addition we have neglected secondary driving forces such as Dufour or Soret effects.

To complete our formulation, a form of the Gibbs-Thomson condition for the interface temperature, $T_i = T(\mathbf{x}_i)$, must be satisfied at the phase boundary. Here we use

$$T_i - T_{\text{sat}} - m\tilde{C}_i + \frac{\gamma(\mathbf{n}) T_{\text{sat}} \kappa}{2L} \left( \frac{1}{\rho_L} + \frac{1}{\rho_G} \right) + \frac{\dot{m}}{\varphi(\mathbf{n})} = 0 \tag{8}$$

where $m$ is the slope of the liquidus line, $\gamma(\mathbf{n})$ and $\varphi(\mathbf{n})$ are the anisotropic surface tension and kinetic mobility, respectively. In Eq. (8) we have neglected the effect of unequal specific heats between phases and ignored the pressure dependence of the melting temperature.

In two-dimensions, the transport equations along with the interface temperature condition, Eq. (8) are solved using the front tracking/finite difference method described in detail by Juric and Tryggvason [12]. Briefly, these equations are solved iteratively for the correct

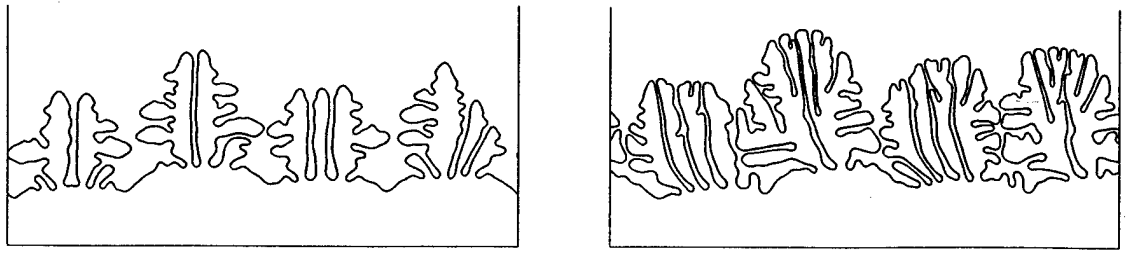

(a) (b)

Figure 1: Comparison of dendritic growth of a pure material (a) with no fluid flow and (b) with fluid flow.

interface velocity, $V_n$, that will satisfy the interface temperature condition, Eq. (8). For the spatial discretization, we use the MAC method of Harlow and Welch [13] with a staggered grid. A first order, phase change projection algorithm, similar to that of Chorin's [14], is used for the time integration. In explicit front tracking, the phase interface is represented discretely by Lagrangian markers connected to form a front which lies within and moves through the stationary Eulerian grid. As the front moves and deforms, interface points are added, deleted and reconnected as necessary throughout the calculation. Thus the interface can exhibit arbitrarily complex interface deformations and topology changes. Information from the integral source terms in Eqs. (2)-(6) are passed between the moving Lagrangian interface and the stationary Eulerian mesh using Peskin's [15] Immersed Boundary Technique. With this technique, the sharp interface is approximated by a smooth distribution function that is used to distribute the sources at the interface over mesh points nearest the interface. Thus the front is given a finite thickness on the order of the mesh size to provide stability and smoothness with no numerical diffusion since this thickness remains constant for all time.

## Computational Examples

We simulated the dendritic growth of a pure material with properties approximately corresponding to that of succinonitrile [16]. The simulations were performed in a 2D, horizontally periodic box of dimensions 11.1 $\times$ 11.1 $\mu$m with an undercooling of -16 K and a 300 $\times$ 300 grid resolution. The solid, attached to the bottom wall, grows upward from an initially perturbed interface. Four-fold anisotropic surface tension provides preferred growth in the horizontal and vertical directions initially. However, rotation of the solid during the calculation can locally change these preferred growth directions. Figure (1a) shows the growth of dendrites into a quiescent liquid. For the situation with flow, Fig. (1b), the density of the solid is no longer equal to the liquid but is roughly 5% greater which results in shrinkage upon solidification and, as can be seen in Fig. (3), a resulting inflow of liquid from the top of the domain. The solid phase was modeled as a liquid of 100 times greater viscosity than the liquid phase. We assumed that the Prandtl number of the material is 1 and also ignored gravity. At the start of the calculation in Fig. (1b) the bottom boundary was given a constant velocity of 41 cm/s. This resulted in a translation of the solid to the right and induces a shear flow within the liquid. At 0.83 $\mu$s the velocity of the bottom boundary was increased to 411 cm/s.

Comparison of Figs. (1a) and (1b) shows that the fluid convection dramatically alters the growth morphology. The presence of flow results in a fuller sidebranch structure and suppresses the emergence of distinct primary dendrite arms. The time evolution of the solid

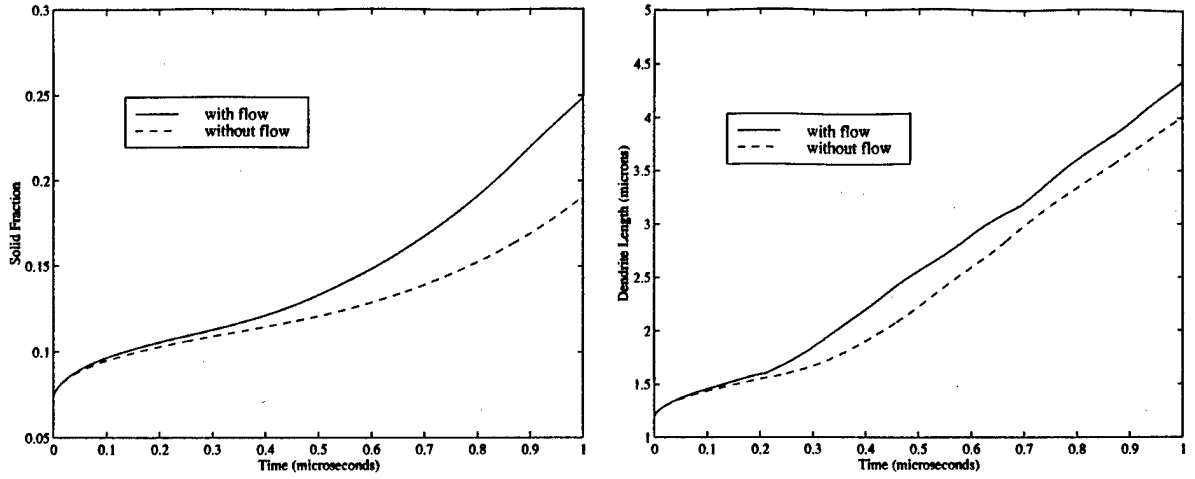


(a) (b)

Figure 2: Comparison of the time evolution of (a) the solid fraction and (b) length of the longest dendrite with time for the cases with flow and without flow in Fig. (1).

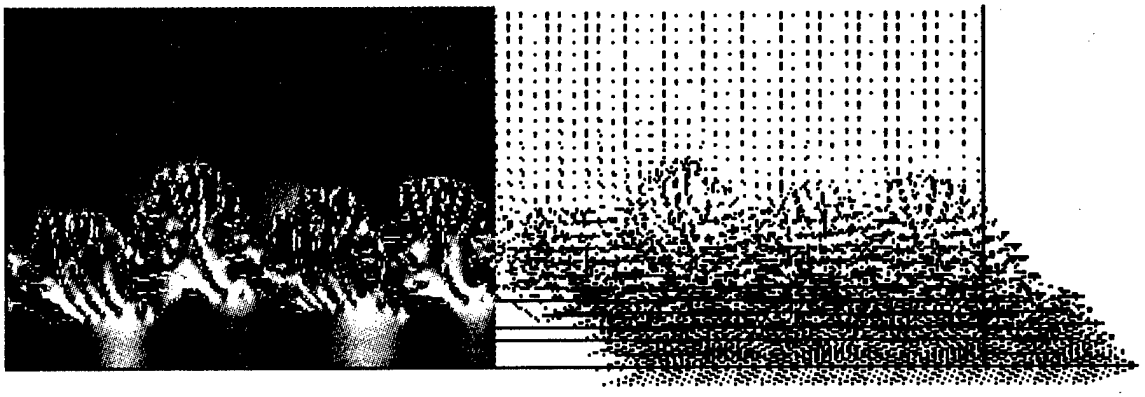

Figure 3: Pressure (left) and velocity (right) fields for the dendritic solidification with flow in Fig. (1b).

fraction and length of the longest dendrite arm are plotted in Fig. (2). As can be seen in Fig. (2a), the shear flow causes the solid to form and fill the domain more rapidly. At 1 $\mu$s, 25% more solid has formed due to the presence of fluid convection. The dendrite tip velocities in the case with flow, inferred from Fig. (2b), are initially greater than the case without flow. However at later times and throughout most of the rest of the calculation, the tip velocities are roughly equal with and without the presence of liquid motion. These gross effects can be attributed to the influence of convection on the thermal envelope of the growing solid. Convection transports cooler liquid into the interstices of the dendritic structure thereby increasing the temperature gradients at the solid/liquid interface which in turn results in larger interfacial growth velocities. Fluid forces also act to bend and deform the dendrites. Figure (3) shows the pressure and velocity fields for Fig. (1). Since the solid is modeled as a viscous liquid the isotropic pressure shows areas where the solid is in tension (light) or compression (dark). Note that the dendrite tips exhibit high pressures due to surface tension.

We next simulated the solidification of globulitic grains of Plutonium alloyed with 1 wt% Gallium [17]. At this concentration, the partition coefficient is 1.37 with a liquidus line

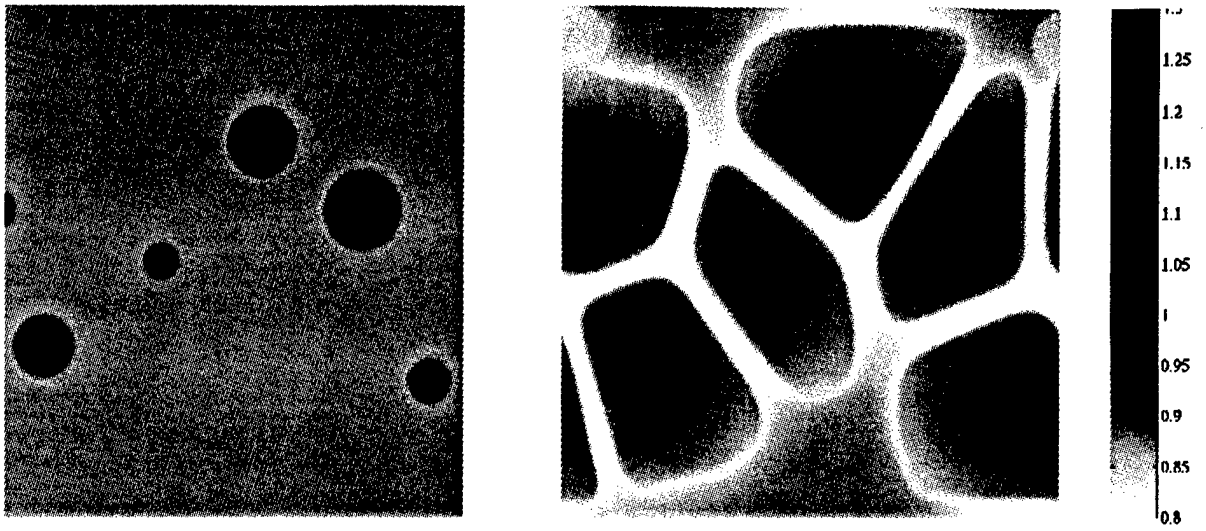


(a) (b)

Figure 4: Solidification of grains of Plutonium - 1 wt% Gallium at (a) $t = 0s$ and (b) $t = 0.375s$.

slope of 37 K/wt%. The liquid diffusion coefficient is 100 times larger than the solid $\epsilon$ phase. The calculation in Fig. (4) begins with six randomly spaced and sized grains of solid $\epsilon$ in a quiescent liquid initially at the melting point of 950 K. We assume that the temperature is spatially uniform and decreases from the melting point at a constant rate of 15 K/min. After 0.375 s the solid grains have grown to fill about 63 % of the 150 $\times$ 150 $\mu$m domain. The color scale shows Gallium concentration in wt% with darker colors indicating higher concentrations. Evident is the coring of the grains with a high Gallium concentration at their centers, decreasing toward the edges. Figure (5) shows the same calculation with an imposed shear flow. Although this calculation is still at an early time, the effect of the flow is to pull the Gallium depleted boundary layers away from the grains. This together with the motion and rotation of the grains within the liquid will result in a very different final concentration distribution.

## Conclusions

We have described a general formulation and method for the direct numerical simulation of solidification microstructures and microsegregation. The method was applied to 2D solidification of pure succinonitrile and a Plutonium-Gallium alloy both with and without the presence of fluid convection. Fluid flow was seen to have an important influence on the morphology and growth dynamics of succinonitrile and the concentration distribution of Gallium.

## Acknowledgments

This work was supported by funding from the Department of Energy/Advanced Strategic Computing Initiative (ASCI). The author wishes to acknowledge helpful discussions with Bruce Murray, Sam Coriell and Geoffrey McFadden of the National Institute of Standards and Technology.

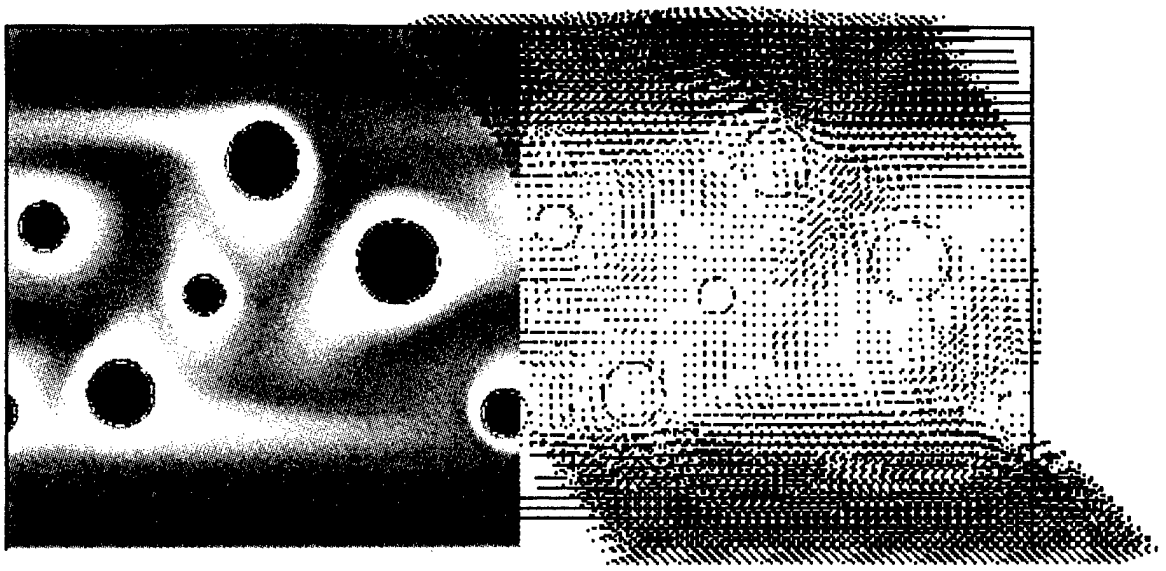

Figure 5: The same calculation as in Fig. (4) with an imposed shear flow. Gallium concentration is plotted on the left and fluid velocities on the right.

## References


[1] K. Tsiveriotis and R. A. Brown, *Int. J. Num. Meth. Fluids,* **16**, pp. 827-843 (1993).

[2] L. H. Ungar, N. Ramprasad and R. A. Brown, *J. Sci. Comput.,* **3**, pp. 77-108 (1988).

[3] A. Schmidt, *J. Comp. Phys.,* **126**, (1996).

[4] R. Kobyashi, *Physica D,* **63**, 410 (1993).

[5] B.T. Murray, A.A. Wheeler and M. E. Glicksman, *J. Cryst. Growth,* **154**, pp. 386-400 (1995).

[6] A. A. Wheeler, W. J. Boettinger and G. B. McFadden, *Phys. Rev. A,* **45**, pp. 7424-7439 (1992).

[7] J. A. Warren and W. J. Boettinger, *Acta Metall.,* **43**, pp. 689-703 (1995).

[8] A. Karma and W.-J. Rappel, *Phys. Rev. Letters,* **77**, pp. 4050-4053 (1996).

[9] D. Juric and G. Tryggvason, *J. Comp. Phys,* **123**, pp. 1-22 (1996).

[10] D. Juric and G. Tryggvason, FED-Vol. 234, (ASME, New York, 1995) pp. 141-148.

[11] H. J. Diepers, C. Beckermann and I. Steinbach, *Solidification Processing 1997,* pp. 426-430.

[12] D. Juric and G. Tryggvason, "Computations of Boiling Flows," to appear in *Int. J. Multiphase Flow.*

[13] F. H. Harlow and J. E. Welch, *Physics of Fluids,* **8**, pp. 2182-2189 (1965).

[14] A. J. Chorin, *Mathematics of Computation,* **22**, pp. 745-762 (1968).

[15] C. S. Peskin, *J. Comput. Phys.,* **25**, 220-252 (1977).

[16] M. E. Glicksman, R. J. Schaefer adn J. D. Ayers, *Metall. Trans. A,* **7**, pp. 1747-1759 (1976).

[17] H. R. Gardner, Battelle-Northwest Report, BNWL-13, UC-25 Metals, Ceramics and Material (TID-4500), 38th Ed.), April, 1965.

Report Number (14) LA-UR--97-3918
CONF-980635--

Publ. Date (11) 199712
Sponsor Code (18) DOE/DP, XF
UC Category (19) UC-706, DOE/ER

DOE